

A molecular dynamics study of the glass transition in $\text{CaAl}_2\text{Si}_2\text{O}_8$: Thermodynamics and tracer diffusion

NEIL A. MORGAN AND FRANK J. SPERA*

Institute for Crustal Studies and Department of Geological Sciences, University of California, Santa Barbara, California 93106, U.S.A.

ABSTRACT

Molecular dynamics (MD) simulation provides a unique window into the microscopic processes controlling the properties of amorphous silicates of geochemical importance. Of special interest are changes in structure and dynamics around the glass transition temperature. Seventeen simulations for composition $\text{CaAl}_2\text{Si}_2\text{O}_8$ in a microcanonical ensemble of 1300 particles (O + Si + Al + Ca) were conducted at temperatures from 1700 to 5000 K at approximately 1 GPa. A pair-wise potential allowing for Coulombic and Born-Mayer interaction was used. Simulation durations were in the range of 50 to 150 ps. Particle trajectories were collected and used to build a picture of the structure and dynamics of equilibrium liquid, supercooled liquid and glassy $\text{CaAl}_2\text{Si}_2\text{O}_8$ as a function of temperature along the 1 GPa isobar. The computer glass transition was detected at $T_g \sim 2800$ K by study of thermodynamic properties, speciation equilibria and tracer diffusivity. T_g is observed as a change in slope of enthalpy (H) vs. temperature at $T = T_g \sim 2800$ K. The configurational isobaric heat capacity of supercooled melt relative to the glass is 53.3 J/(K·mol), within a factor of two of the experimental value. The “computer” isobaric heat capacity for equilibrium liquid at 3000 K is 457 ± 35 J/(K·mol) vs. the calorimetric value of 461 J/(K·mol). In equilibrium liquid, speciation defined by equilibria such as ${}^{11}\text{O} + {}^{13}\text{O} = 2$ ${}^{12}\text{O}$ and $\text{TO}_4 + \text{TO}_6 = 2$ TO_5 are temperature-dependant with ΔH and ΔS approximately equal to -39 kJ/mol and 19 J/mol K and -10 kJ/mol and 12 J/mol, respectively; these are in good agreement with laboratory values. The computer glass point at 2800 K is identified as the temperature at which speciation equilibria become “frozen”. The static structure factor for O-O confirms the conclusion, based on pair correlation statistics, that the glass transition is not associated with significant changes in the static structure. Dramatic differences in the mobility of all atoms monitored by tracer diffusion are noted as a function of temperature. Self-diffusivity orders at fixed temperature according to $D_{\text{Ca}} > D_{\text{O}} > D_{\text{Al}} > D_{\text{Si}}$ with $D_{\text{Ca}} \sim 20\%$ larger than D_{O} and $D_{\text{O}} \sim 2$ D_{Si} . Activation energies for diffusion for all atoms lie in the range 170 to 190 kJ/mol. The small range in tracer diffusivity and activation energy (E_a) found for different atoms suggests cooperative motion is important. At $T_g/T \geq 1$ for the nonequilibrium glass, E_a decreases by $\sim 40\%$ for all atoms compared to corresponding high-temperature (equilibrium melt) values. The crossover between continuous (hydrodynamic-like) motion and atomic hopping motion shows up clearly in the time-dependence of the mean square displacement as a function of temperature. The qualitative view is that a given particle and its neighbors remain trapped for a finite waiting time before undergoing cooperative thermally activated rearrangement. The waiting time distribution is strongly temperature-dependent and related to the rapid increase in structural relaxation time as temperature approaches T_g . Shear viscosity computed from relaxation of microscopic density fluctuations, the Eyring relation and the Green-Kubo formalism are 0.04 Pa·s, 0.09 Pa·s, and 0.02 Pa·s, respectively; these values are all somewhat higher than the extrapolated laboratory value of ~ 0.005 Pa·s.

INTRODUCTION

Glasses constitute a fascinating group of materials from both the fundamental and practical point of view. Although they are amongst the most ancient natural materials used by humans, knowledge of their structure, dynamics and properties remains surprisingly incomplete. Glasses are especially important geological materials. On Earth, rapid cooling of magma produces about 1 cubic kilometer of basaltic glass each year, mainly along

the 70 000-kilometer globe-encircling oceanic ridge system. Global geochemical interchange between hydrosphere, biosphere and lithosphere is influenced by reaction of natural glass with aqueous solutions of varying temperature, pressure and composition. Microbial biofilms develop along the glass-fluid interface and mediate geochemical exchange as well. Glass is also present on other planetary bodies. For example, thermal emission spectrometric data from the Mars Global Surveyor is interpreted to indicate that the Martian lowland in the northern hemisphere (basaltic andesite bulk composition) is dominated

* E-mail: spera@magma.geol.ucsb.edu

by crystals of plagioclase feldspar and volcanic glass (Bandfield et al. 2000). Glass also forms during the ubiquitous process of shock compression during hypervelocity impact of planetary materials. In particular, study of the dynamics, properties and structure of amorphous $\text{CaAl}_2\text{Si}_2\text{O}_8$, is relevant to shock amorphitization and generation of maskelynite. In crystalline form, plagioclase feldspar makes up a substantial part of the lunar crust as well as the oceanic and continental crust on Earth. Melting of subducted plagioclase-rich crust may have played an important role in the Archean and may contribute to island arc volcanism today. High pressure $\text{CaAl}_2\text{Si}_2\text{O}_8$ in the hollandite structure may serve as a repository of elements normally considered incompatible. Additionally, $\text{CaAl}_2\text{Si}_2\text{O}_8$ bears on the distribution of radiogenic heat sources within the Earth's mantle and crystal-liquid partitioning of the large-ion lithophile elements in mantle-derived magma (Zhang et al. 1993; Fodor et al. 1994; Downs et al. 1995; Akaogi 2000). Understanding the nature of glasses, metastable (supercooled) liquids and equilibrium liquids is evidently important for a variety of environmental, geoscience and technological problems.

Despite their ubiquity, some of the most basic questions surrounding amorphous materials remain unanswered. Foremost amongst these is the nature of the transition from equilibrium and supercooled (metastable) liquid to amorphous glassy solid. Glass is an unusual material because it retains the disorder present in normal liquid but shares many macroscopic properties with its corresponding crystalline form. Because many different kinds of materials—from metals to ionic solids to organic polymers to Lennard-Jones fluids—undergo glass transitions, it is clearly a fundamental phenomenon not restricted to a particular class of materials of specific bonding type or composition.

The literature on glasses, structural relaxation, the glass transition and the connection between liquid and glass structure and properties is vast, reflecting its importance. The reviews of Zallen (1983), Hansen and McDonald (1986), Fredrickson (1988), Zarzycki (1991), Binder (1995), Kob (1995, 1999), Debenedetti (1996), Angell (1988, 1991), Angell et al. (1997), Bottinga (1994), Bottinga et al. (1995) and Ediger (1996) are especially informative. Many theories have been proposed to account for the dramatic increase in relaxation time and accompanying strong variation in transport properties such as shear viscosity and tracer diffusion at the glass transition. Since the 1980s, increased interest in the structure, dynamics, and properties of melts and glasses of geochemical importance has arisen. New experimental and computational techniques have been applied to supplement traditional phase equilibria and thermochemical investigations. The review volume edited by Stebbins et al. (1995) presents a comprehensive summary of the structure, dynamics and properties of silicate melts, supercooled liquids and glasses of special relevance to geochemical problems up until that time.

In the present work, the structure and atomic mobility of amorphous $\text{CaAl}_2\text{Si}_2\text{O}_8$ is studied as a function of temperature from 1700 K to 5000 K at a pressure of ~ 1 GPa using the Molecular Dynamics (MD) technique. In particular, we investigate how temperature affects the short range structure of the equilibrium liquid, how the mechanism of diffusion changes

around T_g when speciation equilibria becomes “frozen,” and the role of cooperative motion in thermally activated self diffusion of Si, Al, O, and Ca. In another study (Morgan and Spera, unpublished manuscript, 2001), tagged particle dynamics are used to obtain a detailed microscopic picture of the glass transition and extant theories of viscosity and structural relaxation are discussed in light of insight gained from the MD simulations.

$\text{CaAl}_2\text{Si}_2\text{O}_8$: Previous work and melting relations

AMD study of liquid anorthite at $T = 4000$ K, a temperature well above the “computer” glass transition of $T_g \approx 2800$ K from 1 bar (10^{-4} GPa) to 76 GPa (~ 1800 km depth on Earth) has been presented by Nevins and Spera (1998). This work is briefly reviewed here because of its relevance to the present study. Profound changes in short-range structure and atom mobility were found to occur in molten (fully relaxed) anorthite (i.e., equilibrium liquid) as pressure increases at $T = 4000$ K. This temperature is greater than both the calorimetric and computer glass transition temperatures of 1160 K and ~ 2800 K, respectively. The abundance of TO_4 and TO_6 ($T = \text{Si, Al}$) polyhedra monotonically decrease and increase, respectively, as pressure increases. The concentration of pentahedrally coordinated T ($^{[5]}T$ or TO_5) attains a maximum at 5 GPa. Significantly, at ~ 5 GPa, the tracer diffusivity of both O and Si take on maximum values. Large changes in the O about O and O about T nearest neighbor coordination statistics occur as pressure increases. The former changes rapidly in the 0 to 10 GPa range whereas the latter exhibits a broad peak in $^{[3]}O$ (that is, O with three nearest T neighbors as in the stishovite structure) around 40 GPa. The formation of significant numbers of TO_5 polyhedra drastically alters intermediate range (0.5–1.5 nm) order by frustration of ring formation defined by linkage of corner-sharing TO_4 tetrahedra. These results provide the microscopic basis for the pressure dependence of the macroscopic properties of molten $\text{CaAl}_2\text{Si}_2\text{O}_8$. Because the MD simulations performed by Nevins and Spera (1998) were carried out isothermally, neither the temperature-dependence of short range structure, nor the glass transition were studied. By combining the results presented below with those obtained earlier, one obtains a first-order picture of the microscopic structure of molten $\text{CaAl}_2\text{Si}_2\text{O}_8$ for pressures in the range 0 to 76 GPa and temperatures in the range 2800 to 5000 K.

Amorphous $\text{CaAl}_2\text{Si}_2\text{O}_8$ illustrates classic fragile-liquid behavior (Angell 1985, 1991, 1995). Although stoichiometrically a tetrahedral “2-4” fluid (O in nominal twofold coordination with T ($T = \text{Si, Al}$) and T in fourfold coordination with O), $\text{CaAl}_2\text{Si}_2\text{O}_8$ exhibits marked non-Arrhenian shear viscosity-temperature behavior at low pressure (Fig. 1a). The apparent activation energy for viscous flow at low-temperature is three to five times greater than the corresponding value at high temperatures in the equilibrium liquid. Unlike typical strong network melts, the change in isobaric heat capacity at the calorimetric glass transition, a measure of the configurational entropy of supercooled liquid relative to the crystal at T_g , is relatively large (Fig. 1b). For $\text{CaAl}_2\text{Si}_2\text{O}_8$, Richet and Bottinga (1995) cite $\Delta C_p \approx 8$ J/g atom K at the laboratory glass transition. In contrast, SiO_2 and $\text{NaAlSi}_3\text{O}_8$, both “strong” fluids,

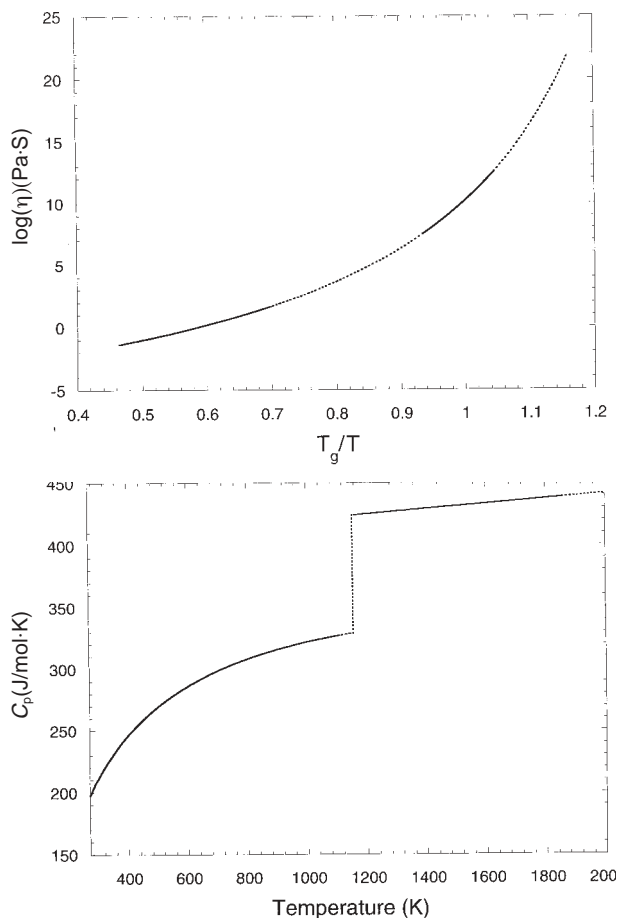


FIGURE 1. (a) Log viscosity (Pa·s) vs. T_g/T for $\text{CaAl}_2\text{Si}_2\text{O}_8$ ($T_g = 2800$ K) from laboratory viscosity data fit to the VTF equation from data compiled by Hummel and Arndt (1985). Solid lines encompass temperature intervals over which laboratory data was fit; dotted lines are interpolated or extrapolated. (b) Laboratory isobaric heat capacity (J/mol·K) for $\text{CaAl}_2\text{Si}_2\text{O}_8$ plotted vs. temperature from parameters provided by Richet and Bottinga (1984b).

exhibit ΔC_p values at $T_g \approx 1480$ K and 1100 K, respectively, of about 2 J/g atom K.

Morse (1980) summarizes the melting of crystalline anorthite. At ~ 1 GPa (the mean pressure of the MD simulations) anorthite melts congruently at 1841 K. Above ~ 1 GPa, anorthite melts incongruently to crystals of corundum (Al_2O_3) plus a liquid more rich in Ca and Si than stoichiometric anorthite. The incongruent melting reaction is $\text{CaAl}_2\text{Si}_2\text{O}_8$ (an) \rightarrow Al_2O_3 (cor) + CaSi_2O_5 (liq). Interestingly, Stebbins and Poe (1999) demonstrate that ^{15}Si , along with octahedral Si is present in CaSi_2O_5 glass quenched from the liquid state at 2575 K and 10 GPa. This is consistent with the simulations of Nevins and Spera (1998) where both ^{15}Si and ^{16}Si were noted.

Computer vs. laboratory glass transition

The phenomenology of structural relaxation and the dependence of the glass transition temperature on cooling rate in labo-

ratory studies has been discussed extensively in the literature (e.g., see Moynihan et al. 1976; Brawer 1985; Scherer 1986; Dingwell 1995). The calorimetric glass transition for $\text{CaAl}_2\text{Si}_2\text{O}_8$ at 10^5 Pa is 1160 K at a cooling rate of $\gamma = 10^{-11}$ K/ps [1 picosecond (ps) = $1 \cdot 10^{-12}$ s] according to Richet and Bottinga (1995) and 1109 K at $\gamma = 1.7 \cdot 10^{-11}$ K/ps according to Moynihan (1995). These values, based on laboratory quench rates, may be compared to the “computer” glass transition found in this study (see below) of $T_g \approx 2800 \pm 200$ K at a quench rate of ~ 700 K/ps, thirteen orders of magnitude faster than the laboratory cooling rate.

The computer T_g for anorthite composition is lower than that for silica of 3050 K and 3300 K for cooling rates of $\gamma = 70$ K/ps and 700 K/ps, respectively, using the BKS potential for silica (Vollmayr et al. 1996; van Beest et al. 1990). In contrast, Della Valle and Andersen (1992) estimate $T_g \sim 2200$ K for silica using the TTAM potential (Tsuneyuki et al. 1988; see also Rustad et al. 1990, 1991a, 1991b, 1991c, 1992). In comparison, the laboratory calorimetric glass transition for silica is ≈ 1480 K (Richet and Bottinga 1995) for $\gamma = 10^{-11}$ K/ps. A useful heuristic is that the ratio of the computer to calorimetric glass transition temperature is ≈ 2.4 (see Bryce et al. 1999 for additional examples in the system $\text{NaAlO}_4\text{-SiO}_2$).

Although the glass transition temperature varies with cooling rate, it is reasonable to believe that the underlying microscopic dynamics of the transition are similar regardless of quench rate. In broad terms, models for the glass transition can be broken into two classes: thermodynamic and nonthermo-dynamic. In the thermodynamic view, the observed glass transition is the kinetic manifestation of an underlying second order Ehrenfest phase transition at the Kauzmann temperature T_K ($T_K < T_g$) with discontinuous derivatives of thermodynamic state variables such as the isobaric expansivity, $\alpha_p [= V^{-1}(\partial V/\partial T)_p]$ and isobaric heat capacity $C_p [= (\partial H/\partial T)_p]$. The vanishing of the entropy difference between metastable (supercooled) liquid and crystalline solid is a consequence of the change in isobaric heat capacity of the material at the Kauzmann temperature, T_K , as new degrees of freedom come into play. In nonthermodynamic theories, structural arrest is viewed purely as a dynamical singularity associated with dramatic growth of relaxation time for decay of microscopic density fluctuations in the supercooled liquid. From this vantage, the glass point marks a transition from ergodic to nonergodic behavior in $6N+1$ -dimensional potential energy-phase space. The hope is that although cooling rate clearly affects the numerical value of T_g , the underlying microscopic dynamics captured by carefully performed Molecular Dynamics simulation is relevant to thermal arrest, the drastic increase in relaxation time on approach to the glassy state and the configurational entropy of fully ergodic liquid.

In the following sections, the structure, properties and dynamics of $\text{CaAl}_2\text{Si}_2\text{O}_8$ at temperatures spanning the glass transition temperature are described. $\text{CaAl}_2\text{Si}_2\text{O}_8$ is expected to exhibit somewhat more complicated behavior than a simple two-atom material such as silica. In $\text{CaAl}_2\text{Si}_2\text{O}_8$, the TO_n network (mainly TO_4 at low pressure) is characterized by equal numbers of Si-O and Al-O bonds, not just Si-O bonds as in silica. There is therefore additional configurational entropy and steric distortion introduced by the mixing of Al and Si of different nominal size and charge. Moreover, the divalent alka-

line earth metal Ca is present in $\text{CaAl}_2\text{Si}_2\text{O}_8$ and missing in silica. The coordination, mobility and possible cooperative motion of O and Ca is a factor missing in compositionally simpler silicates. Finally, unlike the alkali aluminosilicates, where the ratio of Na to O diffusivity is of order 10–100, Ca has about the same tracer diffusivity as O (see below). The multicomponent nature of $\text{CaAl}_2\text{Si}_2\text{O}_8$ complicates the analysis of structural relaxation. At the same time, at least this level of complexity is present in real geofluids and it appears worthwhile to study such systems further despite use of a rather simple form for the potential energy expression.

METHODS

The MD simulations were performed on IBM RS 6000–43P and RS 6000–350 workstations using FORTRAN algorithms developed from Allen and Tildesley (1987) by Rustad et al. (1990) and modified by Stein and Spera (1995, 1996). Self-diffusion, thermodynamic and structural properties were computed from codes developed for this study and by Stein and Spera (1995), Nevins and Spera (1998), and Bryce et al. (1999). A simple pairwise additive intermolecular potential containing Coulomb interactions and exponential Born-Mayer-Huggins repulsion was used: $U_{ij} = q_i q_j / r_{ij} + A_{ij} \exp(-B_{ij} r_{ij})$. The size and softness parameters found in Scamehorn and Angell (1991) have been mapped into the form of A_{ij} and B_{ij} where the full ionic charge between particle i , q_i , and particle j , q_j is separated by the interparticle distance, r_{ij} . Values of the potential parameters are identical to those used by Nevins and Spera (1998). The Ewald method was used to compute the Coulomb interaction for each ion and a cutoff of 8 Å was used in evaluation of repulsive forces. The Gaussian distribution canceling parameter, κ , was set to $5/L$, where L is the length of the primary MD cubic box edge. The sum over the reciprocal lattice vectors $\mathbf{k} = 2\pi/L (\mathbf{k}_x, \mathbf{k}_y, \mathbf{k}_z)$ were determined for $\mathbf{k}_x^2 + \mathbf{k}_y^2 + \mathbf{k}_z^2 \leq 81$. Most simulations were performed with 1300 particles for 50 ps using one femtosecond (fs) time steps in the Verlet algorithm. Two simulations ($T = 2670$ K and 3475 K) were carried out for 150 ps with $N = 1300$ particles to study relaxation at longer times. All production runs were performed in the NVE (microcanonical) ensemble with momentum and energy conserved to greater than one part in 10^5 . NVE stands for a simulation with constant number of particles (N), energy (E), and volume (V). The temperature, pressure, density, energy (total and potential) and simulation durations are listed in Table 1. Typical temperature fluctuations are ~ 50 K while the pressure fluctuations are about 0.7 GPa. The average pressure of all 17 simulations (Table 1) carried out at all temperatures is 1.05 GPa with a standard deviation (1σ) of 0.37 GPa, smaller than pressure fluctuations during single nearly isothermal simulations.

The cooling schedule involved an initial system of 100 Ca, 800 O, and 200 Al and 200 Si ions randomly configured at $T \sim 100\,000$ K. Large intermolecular potential forces were allowed to relax for a period of 10 ps before the system was quenched to 10 000 K at rate $\gamma = dT/dt = 10\,000$ K/ps by velocity scaling. Excess momentum in the system was then removed and the system equilibrated for 10 ps. From 10 000 K, a benchmark configuration at 3000 K and 1.35 GPa was obtained with a

temperature quench rate of 700 K/ps and a pressure quench rate (dP/dt) of 1 GPa/ps. The benchmark-equilibrated configuration at 3000 K was the initial configuration for all production runs. To remain along the isobar, the system was either cooled or heated at a quench rate $\gamma = 70$ K/ps isobarically. Once the desired temperature was achieved and velocity scaling turned off, a 50 or 150 ps NVE production simulation was performed. In sum, three cooling rates were used in this study: one to rapidly cool down the system ($dT/dt = 10^4$ K/ps), a second to reach a benchmark configuration ($dT/dt = 700$ K/ps), and a third to leapfrog from the benchmark temperature to a desired temperature ($dT/dt = 70$ K/ps).

The difference in the benchmark configuration and the leapfrog quench rate raises the issue of how quench rate affect the MD results. It is known that cooling rates have an effect on both the macro and microscopic properties of an amorphous material in simulation experiments (e.g., see Vollmayr et al. 1996). To study the effects of variable quench rate, the 10 000 K momentum-free system was quenched at 70 K/ps (instead of 700 K/ps) to a benchmark temperature of 3000 K; this simulation is denoted in various figures in this paper with the label $\gamma = 70$ K/ps to distinguish it from other runs all of which were quenched at 700 K/ps. A detailed comparison of the properties and structure of the 70 K/ps and 700 K/ps supercooled materials brought to the same final temperature obviated the need for further evaluation because analysis revealed only small differences in structure and properties.

RESULTS

Enthalpy vs. temperature

In Figure 2, molar enthalpy determined from the simulations is plotted against temperature along the ~ 1 GPa isobar. Enthalpy is computed from its thermodynamic definition, $H = E + pV$ where E is the internal energy (sum of potential and kinetic energy), p is the mean pressure of the simulation and V is the molar volume. To highlight the curvature of the computed array, two linear fits are shown: the dashed line is fit using data for $T < 2800$ K and the solid line is fit for $T > 2800$ K. We identify $T_g = 2800 \pm 200$ K as the computer glass transition temperature of $\text{CaAl}_2\text{Si}_2\text{O}_8$ for the quench rate of this study. It is not the goal of this study to precisely define T_g ; rather we are interested in studying changes in properties and structure across the glass transition. In fact, the numerical value of T_g is better constrained by analysis of the dynamics of the transition (Morgan and Spera, unpublished manuscript, 2001). At any rate, here we adopt 2800 K as the computer glass transition temperature.

The slope of the two fit curves gives the isobaric molar heat capacity, $C_p = (\partial H / \partial T)_p$ for $T > T_g$ (≈ 2800 K) and $T < T_g$, respectively. The difference in slope gives the change in isobaric heat capacity between supercooled liquid and computer glass of $\Delta C_p \approx 53$ J/(K·mol) (or 4.1 J/g atom K) at the “computer” glass transition of 2800 K and 1 GPa. The average isobaric heat capacity for all 17 production simulations ($T_{av} = 2941$ K) is 457 ± 35 J/(K·mol) and is independent of temperature. An experimental value of 438 ± 3 J/(K·mol) is reported for supercooled liquid anorthite by Richet and Bottinga (1984a) at $T =$

TABLE 1. Molecular dynamics simulations physical data summary: $\text{CaAl}_2\text{Si}_2\text{O}_8$

T (K)	P (GPa)	ρ (kg/m ³)	Total Energy (kJ/mol)	Potential Energy (kJ/mol)	Duration (picoseconds)
1707.0 ± 29.0	1.32 ± 0.45	2605	-4.246·10 ⁴	-4.274·10 ⁴ ± 7.210·10 ²	50
1871.3 ± 32.8	0.45 ± 0.55	2503	-4.239·10 ⁴	-4.271·10 ⁴ ± 7.443·10 ²	50
2013.6 ± 36.9	1.20 ± 0.51	2559	-4.235·10 ⁴	-4.269·10 ⁴ ± 7.778·10 ²	50
2239.7 ± 39.9	0.88 ± 0.57	2495	-4.227·10 ⁴	-4.265·10 ⁴ ± 7.555·10 ²	50
2320.8 ± 40.7	1.00 ± 0.56	2561	-4.224·10 ⁴	-4.263·10 ⁴ ± 7.412·10 ²	50
2542.3 ± 45.6	1.18 ± 0.59	2553	-4.215·10 ⁴	-4.258·10 ⁴ ± 7.566·10 ²	50
2670.1 ± 49.8	1.04 ± 0.60	2504	-4.212·10 ⁴	-4.256·10 ⁴ ± 7.871·10 ²	150
2868.1 ± 57.5	1.15 ± 0.66	2502	-4.203·10 ⁴	-4.251·10 ⁴ ± 8.478·10 ²	50
2947.5 ± 51.0	0.86 ± 0.65	2448	-4.200·10 ⁴	-4.248·10 ⁴ ± 7.271·10 ²	50
3086.6 ± 59.1	1.03 ± 0.70	2466	-4.194·10 ⁴	-4.245·10 ⁴ ± 8.034·10 ²	50
3150.2 ± 56.5	1.24 ± 0.71	2465	-4.192·10 ⁴	-4.244·10 ⁴ ± 7.539·10 ²	50
3475.3 ± 61.8	1.12 ± 0.71	2458	-4.178·10 ⁴	-4.235·10 ⁴ ± 7.435·10 ²	150
3481.3 ± 61.9	1.17 ± 0.73	2465	-4.177·10 ⁴	-4.234·10 ⁴ ± 7.431·10 ²	50
3983.3 ± 71.5	1.33 ± 0.75	2434	-4.156·10 ⁴	-4.223·10 ⁴ ± 7.469·10 ²	50
4151.6 ± 72.4	0.17 ± 0.78	2465	-4.150·10 ⁴	-4.218·10 ⁴ ± 7.239·10 ²	50
4500.0 ± 40.6	1.88 ± 0.81	2465	-4.135·10 ⁴	-4.208·10 ⁴ ± 3.743·10 ²	50
4976.5 ± 88.5	0.85 ± 0.81	2466	-4.115·10 ⁴	-4.196·10 ⁴ ± 7.324·10 ²	50

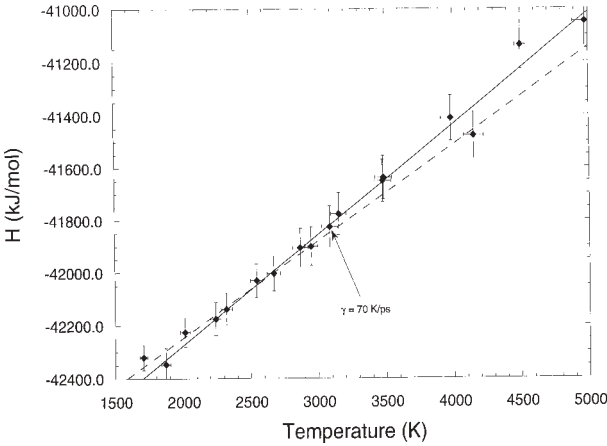


FIGURE 2. Molar enthalpy vs. temperature. Linear fits were made to data for $T > 2800$ K (solid line) and $T < 2800$ K (dashed) where $T_g = 2800$ K. The MD-computed configurational isobaric heat capacity for supercooled $\text{CaAl}_2\text{Si}_2\text{O}_8$ is the difference between the high-temperature and low temperature slope in H - T coordinates.

1800 K. Above the calorimetric glass transition, the isobaric molar heat capacity of supercooled $\text{CaAl}_2\text{Si}_2\text{O}_8$ (metastable liquid) is $C_p = 400.77 + 20.24 \cdot 10^{-3} T$ J/(K·mol) which gives $C_p = 461$ J/(K·mol) at 3000 K in good agreement with the MD value of 457 ± 35 J/(K·mol).

Although MD can capture a change in the heat capacity of about the right magnitude (within a factor of two of the laboratory value), the transition based on ΔC_p is somewhat “smeared out.” A more refined view of the glass transition is gained by examining dynamical properties such as tracer diffusion and shear viscosity. Before turning to these, the effect of temperature on the short-range structure of molten anorthite is studied. Recall that T_g may be thought of as the characteristic temperature at which metastable supercooled liquid becomes a nonequilibrium glass.

Short range structure of molten and glassy anorthite

The dependence of short range ($r < 0.5$ nm) structure at $1700 \text{ K} < T < 5000 \text{ K}$ and ~ 1 GPa has been studied. Although at $T < T_g$ short range structures vary comparatively little, this is distinctly not the case for the equilibrium liquid at $T > 2800$ K. It is easy to develop a thermodynamic model to describe the short range order or “speciation” in molten $\text{CaAl}_2\text{Si}_2\text{O}_8$ by analysis of coordination statistics. These results can be compared with spectroscopic and phase equilibria data to gain some idea of the quality of the potential used in the simulations.

The coordination number (CN) of any atom about any other is found by numerical integration of the pair correlation function from zero to the to the first minimum in the partial pair correlation defined:

$$g(r) = \frac{V}{N^2} \left\langle \sum_{i=1}^N \sum_{j=1}^N \delta(r - r_{ij}) \right\rangle \quad (1)$$

For two atoms, i and j , where V is the volume of the MD primary box and N is the number of particles, $g_{ij}(r)$ finds the normalized distribution of one atom around another within a defined cut-off distance. In computing the coordination statistics, slight variations in the first minimum of (1) were taken into account for each simulation due to variations with temperature.

The temperature dependence of the coordination of T about O in $\text{CaAl}_2\text{Si}_2\text{O}_8$ system, where T is either Si or Al, is shown in Figure 3a. Although we have studied both Si and Al coordination statistics individually, we group Al and Si together when showing results in this study because the differences remain rather small at least for the range in pressure, temperature and quench rate examined here. Nevins and Spera (1998) have studied fractionation of Al and Si in TO_n polyhedra as a function of pressure and their results are consistent with the small effects seen in the present study.

An O atom bonded to a single T atom is labeled ^{11}O , ^{12}O is an O atom with the two nearest T neighbors, ^{13}O is an O atom coordinated with three T atoms (as in the stishovite structure), and so on. Across the temperature range studied, O speciation is dominated by ^{12}O and ^{13}O ($\sim 90\%$ of the total). The concentration of ^{11}O is always less than 10% and ^{14}O is present at

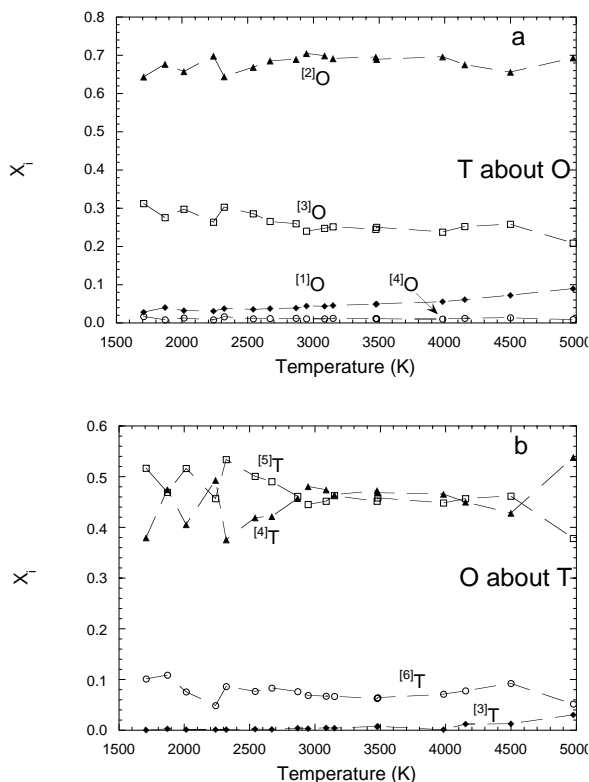


FIGURE 3. Short range coordination statistics for $\text{CaAl}_2\text{Si}_2\text{O}_8$ at 1 GPa. (a) Number fraction of T ($T = \text{Si}, \text{Al}$) about O atom vs. temperature. A weak dependence of coordination number with temperature exists for $T > 2800$ K. (b) Number fraction of O atoms about T vs. temperature. A weak dependence is noted for $T > 2800$ K but no significant short-range differences in structure occur around the computer glass transition.

defect levels (several percent at most). A nominal temperature dependence can be seen in the increase of $^{[1]}\text{O}$ from $\sim 3\%$ at 1707 K to $\sim 10\%$ at 4980 K (note that most of the change occurs for $T > \sim 2800$ K) and a concomitant decrease of $^{[3]}\text{O}$ from 31% to 20% over the same temperature interval. $^{[4]}\text{O}$ varies little and $^{[2]}\text{O}$ fluctuates gently around 67%, nearly constant within the limits of resolution. The observed effect of temperature, although systematic, is quite small. Most importantly, there are no remarkable changes in short-range structure around T_g .

In Figure 3b, the coordination of O atoms around T ions is considered. The T ions are mostly four and five fold coordinated ($^{[4]}\text{T}$ and $^{[5]}\text{T}$). The abundance of $^{[4]}\text{T}$ and $^{[5]}\text{T}$ (both potential ring formers) inversely correlate over the temperature range from 53% $^{[5]}\text{T}$ and 46% $^{[4]}\text{T}$ at 2320 K to 38% $^{[5]}\text{T}$ and 52% $^{[4]}\text{T}$ at 4976 K. The abundance of TO_6 polyhedra is constant around 10%. There is no indication of any structural discontinuity near the glass transition.

The coordination of O atoms about Ca is shown in Figure 4a. Five different coordination polyhedra (from five to nine fold) are found greater than a few percent by number concentration. At low temperature, $^{[6]}\text{Ca}$, $^{[7]}\text{Ca}$, and $^{[8]}\text{Ca}$ are the most common with an average coordination number (CN) of 6.6. A weak temperature dependence is apparent with a tendency to-

ward lower CN as the temperature increases; at ~ 5000 K the average CN for O about Ca is 5.8 and the predominant CNs are 5, 6, and 7.

Calcium about O coordination exhibits virtually no variation over the temperature range studied (Fig. 4b). Approximately 70% of the O atoms have a single Ca nearest neighbor and about 25% have two nearest Ca neighbors. Less than 5% of the O atoms have three or more nearest Ca neighbors. Figure 4 portrays little, if any, temperature-dependence and no indication of discontinuity in short-range order of Ca about O near T_g .

In Figure 5, CNs of O atoms about O atoms vs. temperature are shown. The O about O coordination exhibits some fluctuation with temperature although the average O about O CN hardly changes (i.e., at 1700 K, $\text{CN} \approx 9.2$ whereas at 4900 K, $\text{CN} \approx 8.7$). Between 2500 K and 3500 K, $^{[6]}\text{O}$, $^{[7]}\text{O}$, $^{[8]}\text{O}$, and $^{[9]}\text{O}$, increase, whereas $^{[10]}\text{O}$, $^{[11]}\text{O}$, and $^{[12]}\text{O}$ decrease. The small change in the average CN from 9.2 to 8.7 reflects the small expansion of the network as temperature increases.

The distribution of local coordination of Si about Al, Si about Si, Al about Al, and Al about Si was also determined. For Si, the distribution is fairly broad with about 70% of the Si atoms

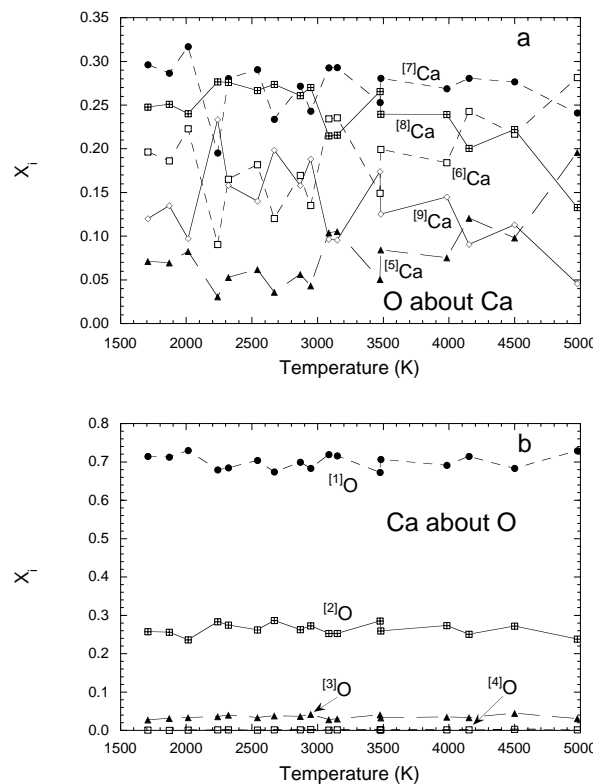


FIGURE 4. Short range coordination statistics for $\text{CaAl}_2\text{Si}_2\text{O}_8$ at 1 GPa. (a) Number fraction of O atoms about Ca atoms vs. temperature displaying little temperature dependence except for a slight decrease in average coordination number (CN) with increasing temperature due to lengthening of Ca-O bond distances. (b) Number fraction of Ca atoms about O atoms vs. temperature. There is little variation across the temperature interval investigated.

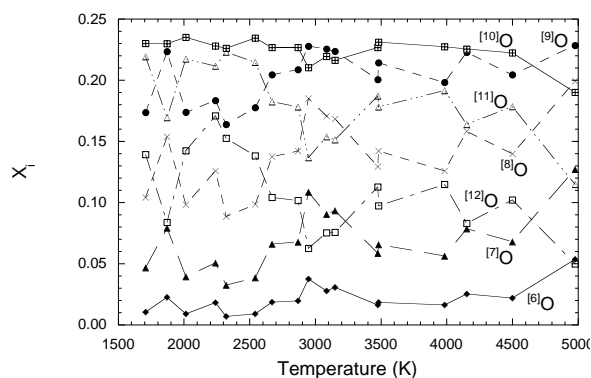


FIGURE 5. Short range coordination statistics for $\text{CaAl}_2\text{Si}_2\text{O}_8$ at 1 GPa. Number fraction of O atoms about O atoms vs. temperature. The mean CN of O atoms about O atoms decreases from 9.2 to 8.7 between 1700 K and 5000 K indicating bond lengthening at high temperatures in the equilibrium liquid.

having between two and four nearest neighbors of Al whereas 80% of the Si atoms have between one and three nearest neighbors of Si. For Al, the distribution is somewhat broader with 70% having between two to five nearest neighbors of Al atoms and about 70% having between two to four nearest neighbors of Si atoms. No systematic changes in T about T coordination occurred in the temperature range studied.

In summary, changes in short range order as monitored by coordination statistics of O about T, T about O, O about Ca, Ca about O, O about O, and T about T at temperatures around T_g are not marked. This result is consistent with MD studies on Lennard-Jones systems, ionic fluids as well as covalent materials such as silica (e.g., see Kob 1999) and indicates the glass transition is not a strictly static structural transition. Note that in contrast, at temperature above T_g , coordination statistics for Si and Al about O and for O about Si and Al do vary systematically. This implies attainment of equilibrium on time scales less than 50 ps at 3500 to 5000 K and 1 GPa.

Thermodynamic model for O and TO_n coordination

If we accept the observed systematic differences in speciation with temperature for $T > T_g$ as representative of different liquid equilibrium states, it is possible to compute the enthalpy and entropy of appropriate speciation reactions. These can then be compared with determinations based on IR and NMR spectroscopy and calorimetric data (e.g., Stebbins 1995; McMillan and Wolf 1995; Navrotsky 1995; Hess 1995). Good agreement would provide some confidence in the quality of the potential despite its simple form.

The equilibrium constant for the reaction ${}^{[1]}\text{O} + {}^{[3]}\text{O} \leftrightarrow 2{}^{[2]}\text{O}$ may be written as $K_O = [{}^{[2]}\text{O}]^2 / [{}^{[1]}\text{O}][{}^{[3]}\text{O}]$ where the bracketed quantity refers to the concentration (number fraction) of the particular coordination state of O with respect to T atoms. Similarly, for the reaction $\text{TO}_4 + \text{TO}_6 \leftrightarrow 2\text{TO}_5$ the equilibrium constant $K_T = [\text{TO}_5]^2 / [\text{TO}_4][\text{TO}_6]$ may be written. If we assume that the change in isobaric heat capacity is identically zero for both reactions (a good assumption at these temperatures), then standard thermodynamic analysis gives $\Delta G = 0 = \Delta H^\circ - T\Delta S^\circ + RT$

In K at equilibrium along the 1 GPa isobar. A plot of $\ln K$ vs. $1/T$ enables one to compute the enthalpy and entropy of the O and TO_n speciation equilibria, respectively assuming ideal mixing of the structural entities. In Figure 6a and 6b equilibrium constants are plotted against reciprocal temperature for these speciation reactions. It is noted that a change in regime occurs at $T \approx 2800$ K separating an equilibrium region from a nonequilibrium (frozen) one. A linear fit was made to two parts of the data; one fit for temperatures >2800 K (liquid region) and another for $T < 2800$ K (glassy region). High-temperature (liquid) data gives: $\Delta H^\circ = -38.9$ kJ/mol and $\Delta S^\circ = 18.96$ J/mol K for the O speciation equilibrium. Below T_g , the enthalpy is essentially zero. While there is no structural change at T_g , the “falling out” of equilibrium is clearly reflected in the variation of K_O with temperature. In Figure 6b, TO_n equilibrium speciation data are plotted. In the high-temperature region, $\Delta H^\circ = -10.24$ kJ/mol and $\Delta S^\circ = 12.23$ J/mol K. Again note that ΔH° is approximately independent of temperature below $T_g \approx 2800$ K. To summarize, speciation is essentially “frozen” at T_g for both reactions.

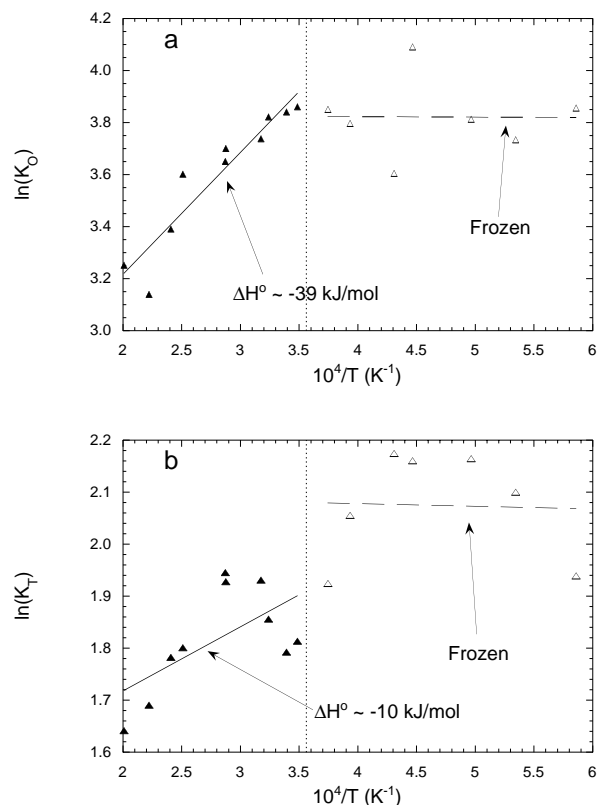


FIGURE 6. O and TO_n speciation equilibria. (a) $\ln K_O$ (see text for definition) vs. $1/T$ for the reaction: ${}^{[1]}\text{O} + {}^{[3]}\text{O} \leftrightarrow 2{}^{[2]}\text{O}$. The enthalpy and entropy of O speciation equilibrium are -39 kJ/mol and 19 J/(mol·K), respectively for equilibrium and metastable liquid ($T > 2800$ K). Below T_g , the equilibrium is frozen (b) $\ln K_T$ (see text for definition) vs. $1/T$ for the reaction: $\text{TO}_4 + \text{TO}_6 \leftrightarrow 2\text{TO}_5$. The enthalpy and entropy of TO_n reaction are -10 kJ/mol and 12 J/(mol·K), respectively for $T > 2800$ K. At $T < 2800$ K TO_n equilibrium is frozen ($\Delta H^\circ = 0$).

Several workers have studied speciation in molten alkali and alkali aluminosilicates silicates as a function of temperature by calorimetric and spectroscopic methods (e.g., Maekawa et al. 1991; Navrotsky 1995; Hess 1995; Stebbins 1995). Typical reaction enthalpies for the O speciation reaction (i.e., K_O) lie in the range -30 to -70 kJ/mol; precise values depend on the nature of the metal oxide as well as the silica/metal oxide ratio. For the reaction $^{10}\text{O} + ^{12}\text{O} \leftrightarrow 2^{11}\text{O}$ with H as the network modifier Ramano et al. (1995) found an enthalpy -36.5 ± 5 kJ/mol which agrees very well with the MD result, $\Delta H^\circ = -38.9$ kJ/mol. Similar values are noted in calorimetric and spectroscopic studies of CaO-SiO_2 and $\text{CaO-Al}_2\text{O}_3\text{-SiO}_2$ melts at temperatures above the laboratory glass transition temperature (Hess 1995). The relatively large positive change in entropy for both speciation reactions is consistent with the larger molar volumes of ^{12}O and TO_3 compared to other coordination environments for O and T atoms (e.g., ^{13}O and TO_6). Finally, we speculate that the enthalpy of the O speciation reaction $^{n-1}\text{O} + ^{n+1}\text{O} \leftrightarrow 2^{n}\text{O}$ for $n > 1$ may be ≈ 35 kJ/mol, a sort of universal value. Studying silicate compositions with different NBO/T (NBO = nonbridging oxygen atoms) ratios can easily test this idea.

Static structure factor

The partial static structure factor for O $S_{\text{Oo}}(\mathbf{k})$ is defined

$$S_{\text{Oo}}(k) = 1 + 4\pi \frac{N_{\text{O}}}{V} \int_0^\infty (g_{\text{Oo}}(r) - 1) \frac{\sin(kr)}{kr} r^2 dr \quad (2)$$

where N_{O}/V is the number volume of O and $g_{\text{Oo}}(r)$ is the O-O pair correlation function. $S_{\text{Oo}}(\mathbf{k})$ measures the spatial dependence of the O density at the nanoscale and provides an overview of structural variations as temperature decreases and passes through the glass transition. In Figure 7, the partial structure factor for O is plotted vs. wavevector \mathbf{k} for temperatures spanning the range of the MD experiments. Most of the power in the O-O static density correlation is at $\mathbf{k}_0 = 2.64 \text{ \AA}^{-1}$. This corresponds to a distance $r \sim 2\pi/\mathbf{k}_0 = 2.38 \text{ \AA}$, essentially equal to the distance of the first peak of the O-O pair correlation function, $g_{\text{Oo}}(r)$. For \mathbf{k} less than about 1.5 \AA^{-1} , the structure is not meaningfully resolved since of the cutoff used in the computation of forces was 8 \AA (Boon and Yip 1980). The important conclusion drawn from Figure 7 is that the static structure factor varies only subtly with temperature. This underscores the conclusion based on short range pair coordination statistics that significant changes in the static structure, such as would occur at a first-order phase transition, do not take place around the glass transition temperature.

In summary, although there are no significant changes in short range structure as T_g is approached, the onset of thermal arrest is easily spotted by the inability of the supercooled liquid to maintain internal equilibrium at temperatures below ~ 2800 K for the time scales probed by the MD simulations. This is the temperature at which the supercooled liquid becomes a “frozen” (nonequilibrium) material (i.e., a glass).

Tracer diffusivity

Transport properties such as tracer diffusion and viscosity exhibit dramatic changes as T_g is approached. It is instructive

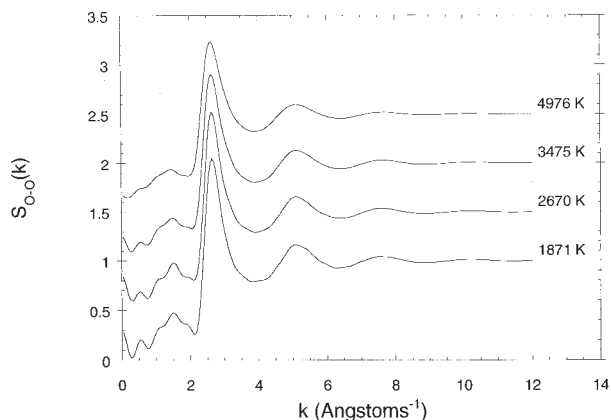


FIGURE 7. Partial static structure factor $S_{\text{Oo}}(\mathbf{k})$ vs. wavevector at temperatures spanning the transition from equilibrium liquid to nonequilibrium glass. Large amplitude peak at 2.64 \AA^{-1} corresponds to the first peak in the O-O pair correlation maximum at about 2.38 \AA .

to examine the mobility of atoms as a function of temperature. Tracer diffusivity (D_i) for each atom may be computed from the mean square displacement (MSD) of a particle averaged for all particles of the same type over the duration of the simulation. Using the Einstein relation, tracer diffusivity for the i^{th} ion is defined:

$$D_i = \lim_{t \rightarrow \infty} \frac{\langle |\mathbf{r}_i(t) - \mathbf{r}_i(0)|^2 \rangle}{6t} \quad (3)$$

where the numerator is the MSD for the i^{th} ion and the brackets imply ensemble averaging. Tracer diffusivity for Ca, Al, Si and O at 1700 to 5000 K are collected in Table 2 and plotted in Figure 8. Reported D_i for $T < 2670$ K represent lower bounds for self diffusion in the nonequilibrium glass (see Fig. 9). For D_i to be meaningful, the MSD must be greater than interatomic distances, e.g., $\text{MSD} > 1 \text{ \AA}^2$. At a given temperature, $D_{\text{Ca}} > D_{\text{O}} > D_{\text{Al}} > D_{\text{Si}}$; D_{Ca} is $\sim 20\%$ larger than D_{O} which, in turn, is about a factor of two larger than D_{Si} . Diffusivities are similar to within a factor of 2 to 3 throughout the temperature range of the simulations. The self-diffusion of Al exceeds that of Si but is smaller than that for O. The overall similarity of all tracer diffusivities at a given temperature suggests that cooperativity plays a role in their collective mobility (Pakula and Teichmann 1997; Lesher et al. 1996; Bryce et al. 1999). Examination of Figure 8 reveals that at $T_g/T \approx 1$ there is a break in slope for all atoms. The energy of activation for diffusion decreases around T_g for all species. The greater scatter of the low temperature data is a reflection of smaller MSDs at lower temperatures with larger statistical uncertainties.

At temperatures above T_g (≈ 2800 K), diffusivity data for each species was fit to the Arrhenian expression $D = D_0 \exp(E_a/RT)$ to obtain activation energies applicable to the liquid. These are collected in Table 3 where it is noted that E_a lies in the restricted range 170 to 190 kJ/mol. Estimated uncertainties for E_a are circa 15 to 20 kJ/mol; the tight grouping of activation energy for the different atoms is consistent with the notion that cooperativity plays a role in tracer diffusion in this system. A fit of diffusion data for all species above and below T_g

TABLE 2. Tracer diffusivity (D_i) for Ca, Al, Si, and O (m^2/s)

T (K)	D_{Ca}	D_{Al}	D_{Si}	D_{O}
1707.0	$7.338 \cdot 10^{-12}$	$4.302 \cdot 10^{-12}$	$3.458 \cdot 10^{-12}$	$8.053 \cdot 10^{-12}$
1871.3	$1.783 \cdot 10^{-11}$	$5.334 \cdot 10^{-11}$	$1.282 \cdot 10^{-11}$	$2.450 \cdot 10^{-11}$
2013.6	$5.569 \cdot 10^{-11}$	$2.071 \cdot 10^{-11}$	$1.679 \cdot 10^{-11}$	$3.449 \cdot 10^{-11}$
2239.7	$7.203 \cdot 10^{-11}$	$1.790 \cdot 10^{-11}$	$1.732 \cdot 10^{-11}$	$4.942 \cdot 10^{-11}$
2320.8	$8.531 \cdot 10^{-11}$	$4.035 \cdot 10^{-11}$	$2.787 \cdot 10^{-11}$	$7.943 \cdot 10^{-11}$
2542.3	$2.188 \cdot 10^{-10}$	$9.030 \cdot 10^{-11}$	$7.704 \cdot 10^{-11}$	$1.451 \cdot 10^{-10}$
2670.1	$1.478 \cdot 10^{-10}$	$7.541 \cdot 10^{-11}$	$5.080 \cdot 10^{-11}$	$1.555 \cdot 10^{-10}$
2868.1	$3.148 \cdot 10^{-10}$	$2.254 \cdot 10^{-10}$	$1.425 \cdot 10^{-10}$	$3.095 \cdot 10^{-10}$
2947.5	$4.830 \cdot 10^{-10}$	$2.399 \cdot 10^{-10}$	$1.315 \cdot 10^{-10}$	$4.063 \cdot 10^{-10}$
3086.6	$5.949 \cdot 10^{-10}$	$3.435 \cdot 10^{-10}$	$1.983 \cdot 10^{-10}$	$4.543 \cdot 10^{-10}$
3150.2	$9.300 \cdot 10^{-10}$	$5.386 \cdot 10^{-10}$	$3.370 \cdot 10^{-10}$	$7.236 \cdot 10^{-10}$
3475.3	$1.703 \cdot 10^{-9}$	$8.602 \cdot 10^{-10}$	$5.567 \cdot 10^{-10}$	$1.174 \cdot 10^{-9}$
3481.3	$1.167 \cdot 10^{-9}$	$1.132 \cdot 10^{-9}$	$7.062 \cdot 10^{-10}$	$1.351 \cdot 10^{-9}$
3983.3	$3.157 \cdot 10^{-9}$	$2.118 \cdot 10^{-9}$	$1.356 \cdot 10^{-9}$	$2.612 \cdot 10^{-9}$
4151.6	$3.319 \cdot 10^{-9}$	$2.557 \cdot 10^{-9}$	$1.726 \cdot 10^{-9}$	$3.113 \cdot 10^{-9}$
4500.0	$4.605 \cdot 10^{-9}$	$3.568 \cdot 10^{-9}$	$2.358 \cdot 10^{-9}$	$4.283 \cdot 10^{-9}$
4976.5	$9.264 \cdot 10^{-9}$	$4.741 \cdot 10^{-9}$	$3.505 \cdot 10^{-9}$	$5.848 \cdot 10^{-9}$

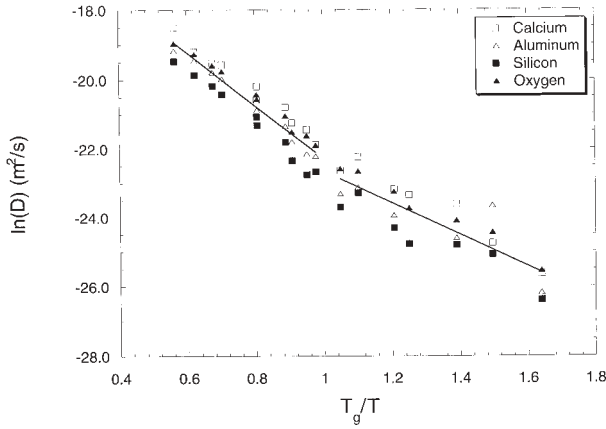


FIGURE 8. Tracer diffusivity. $\ln(D)$ vs. T_g/T with $T_g = 2800$ K for Ca, Al, Si, and O. Least squares fit (all atoms) for $T > 2800$ K and $T < 2800$ K are $\ln D = -14.61 - 7.68 (T_g/T)$ and $\ln D = -18.06 - 4.54(T_g/T)$, respectively. Activation energies are 178 kJ/mol ($T > T_g$) and 107 kJ/mol ($T < T_g$), respectively. Arrhenian parameters for each atom are given for $T > 2800$ K in Table 3.

gives average apparent activation energies of 178 kJ/mol and 107 kJ/mol, respectively (Fig. 8).

Finally, in Figure 9 MSD is plotted vs. the logarithm of time for Ca, Si and O. Three distinct transport regimes are noted. At very short times, atoms move along “ballistic” paths for which inertial scaling gives $\text{MSD} \sim t^2$. This behavior is seen in Figure 9 for all simulations at all temperatures ($T = 1700\text{--}5000$ K) out to ~ 0.2 ps. At greater times, $\text{MSD} \sim t^\beta$ with $0 \leq \beta \leq 1$ and $\beta = f(T)$. For temperature and time where $\beta < 1$, a “sub-diffusive” regime is clearly identified. This regime is associated with the nonequilibrium glass and stands in sharp dynamical contrast to atom mobility in the normal liquid for which $\beta = 1$.

At high temperatures in equilibrium liquid range ($T \gg T_g$), $\text{MSD} \sim 6Dt$. This is expected and clearly observed on Figure 9 even for Si, the least mobile atom (Fig. 9b). As T decreases toward T_g , a plateau region of anomalous sub-diffusion devel-

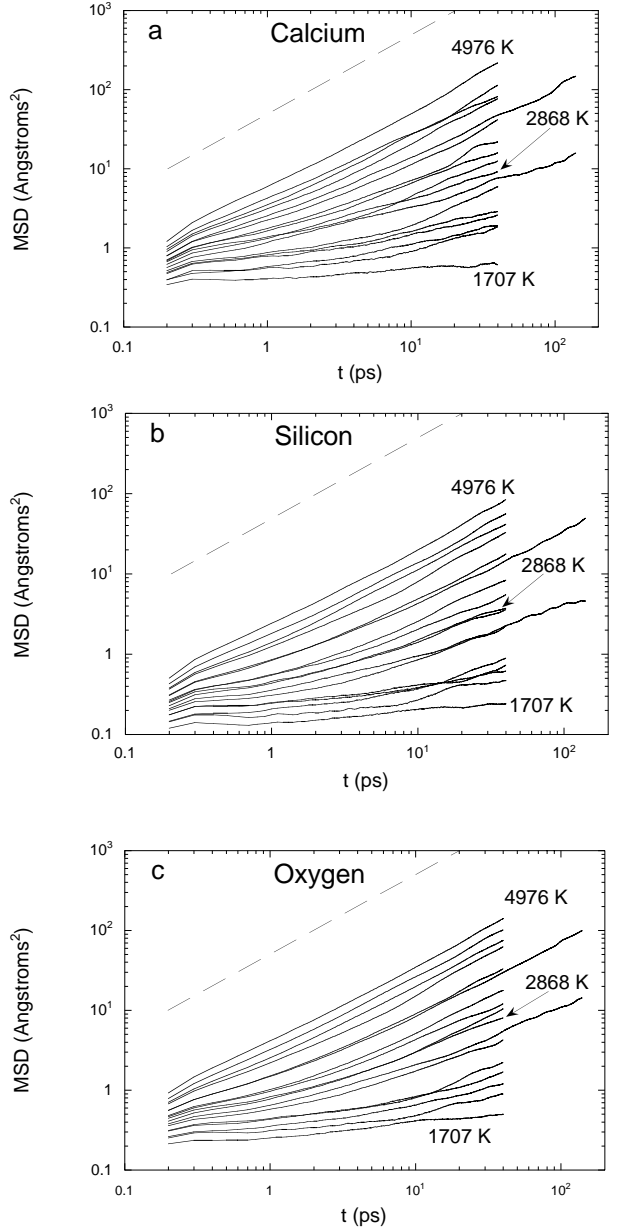


FIGURE 9A–C. Logarithmic plot of the MSD vs. time to illustrating the ballistic, sub-diffusive and diffusive regime (see text). Temperatures of unmarked curves may be found from Table 1.

ops. This is noted as a positive upward curvature of the MSD and becomes accentuated at low temperatures. For example, at 1707 K a well-developed plateau is apparent for Si in the time interval 0.3 to 3 ps. At any given temperature, we expect the power law exponent β goes to unity in the limit $t \rightarrow \infty$. The time at which $\beta \rightarrow 1$ increases dramatically as the simulation temperature decreases. At ~ 5000 K, the hydrodynamic diffusion result $\text{MSD} \sim t$ is attained immediately following the inertial (ballistic) regime. In contrast, for the low temperature simulations, the sub-diffusive regime is maintained up to times exceeding the duration of the simulations. A schematic microscopic interpretation of this feature for O may be offered. Con-

TABLE 3. Arrhenius parameters fit for $T > 2800$ K for tracer diffusivities

Element	$\ln D_0$	E_a (kJ/mol)	R^2
Ca	-14.37	-174.6	0.979
Al	-14.62	-180.5	0.983
Si	-14.70	-191.3	0.982
O	-14.75	-168.5	0.989

Note: D_0 in squared meters per second.

finement of O atoms to cages becomes increasingly important as temperature drops. That is, more of the O finds itself temporarily trapped in cages defined by the O and T sub-lattices. The vibration of caged O atoms in this trapped mode contributes little to its displacement. As temperature increases, distinguishing the rapid oscillatory motion of an O atom within a trap or cage from the random walk (hopping) motion becomes increasingly difficult as the cage life time sharply decreases and becomes ill defined. At high temperatures, the drift of the cage itself is of the same order as the MSD of an O atom performing an uncorrelated random walk and the scaling $\text{MSD} \sim t$ ($\beta = \text{unity}$) is recovered.

In summary, diffusion at high temperatures within the hydrodynamic regime appears to be cooperative characterized by a small range in both the magnitude of the diffusivity and in its temperature-dependence as measured by the activation energy. As T decreases, diffusion becomes anomalous (non-hydrodynamic) with the mean square displacement proportional to some fractional power of time ($\beta < 1$). In microscopic terms, an atom remains trapped at a given position for a finite waiting or residence time before undergoing an activated hop. One may anticipate that the waiting time distribution is strongly temperature-dependent and related to the dramatic increase in relaxation time as temperature approaches T_g .

Shear viscosity

There are several ways to assess the viscosity of liquid $\text{CaAl}_2\text{Si}_2\text{O}_8$ from MD trajectories. Here we estimate the shear viscosity of equilibrium $\text{CaAl}_2\text{Si}_2\text{O}_8$ at 3480 K and 1 GPa using three different methods and compare with extrapolated laboratory data at 1 bar.

The simplest way to determine viscosity is to estimate the Maxwell shear relaxation time from an appropriate correlation and use this relaxation time with the laboratory value of the rigidity modulus. A timescale $\tau \approx 4$ ps is identified as the Maxwell shear relaxation time for molten $\text{CaAl}_2\text{Si}_2\text{O}_8$ at $T \sim 3480$ K based on the decay of microscopic O density fluctuations (Morgan and Spera, unpublished manuscript 2001). A shear viscosity $\eta \sim 0.04$ Pa·s is calculated from the relation $\eta = \tau G_\infty$ where G_∞ is the instantaneous (elastic) shear modulus of glassy anorthite from laboratory experiment (~ 10 GPa, Bansal and Doremus 1986, Dingwell and Webb 1990).

A second independent estimate of the shear viscosity can be made from the Eyring relation $\eta = kT/D_0\sigma$, where σ is the distance to the first minimum of the O-O radial distribution function (~ 0.39 nm) and D_0 is the O tracer diffusivity at 3480 K. This leads to $\eta = 0.09$ Pa·s for the shear viscosity at 3480 K and 1 GPa about a factor of two higher than the estimate made from Maxwell relaxation

Finally, the shear viscosity may be calculated using standard Green-Kubo linear response theory for the decay of the equilibrium stress autocorrelation function (e.g., Ogawa et al. 1990; Horbach and Kob 1999). The relevant Green-Kubo expression is:

$$\eta = \frac{V}{k_B T} \int_0^\infty \langle P_{\alpha\beta}(t) P_{\alpha\beta}(0) \rangle dt \quad (4)$$

where $\langle P_{\alpha\beta}(t) P_{\alpha\beta}(0) \rangle$ is the autocorrelation function of the microscopic stress, k_B is Boltzmann's constant and V is the volume of the primary box (Allen and Tildesley 1987). Because there are three independent off-diagonal components of the shear stress (P_{xy} , P_{xz} , P_{yz}), one obtains three independent estimates of the shear viscosity from the Green-Kubo formalism. The average of the three values is 0.023 ± 0.008 Pa·s at 3480 K and 1.1 GPa and the quoted error is the 2-standard deviation.

The viscosity computed from the Maxwell relaxation time and Green-Kubo formalism agree to within a factor of two whereas the G-K and Eyring viscosity agree to a factor of four. Although the viscosity of molten anorthite has not been measured at 3500 K and 1 GPa, one may obtain an estimate based on Arrhenian extrapolation of high temperature (~ 2000 K) laboratory measurements of Urbain et al. (1982) at 1 bar. This procedure gives $\eta = 0.005$ Pa·s but it is not possible to estimate the uncertainty given the rather large extrapolation. Using a VTF (Vogel-Tammann-Fulcher) rather than Arrhenian form to fit the Urbain data one finds $\eta = 0.004$ Pa·s which is not significantly different. The discrepancy between the laboratory and MD computed values can not be ascribed to the effects of pressure because, as shown by Nevins and Spera (1998), in the range zero to 1 GPa we expect the viscosity to decrease as pressure increases along the isotherm. Possible causes of the discrepancy include experimental error, an inaccurate potential or sampling error associated with too few particles in the MD simulations.

CONCLUDING REMARKS

Because MD quench rates are many orders of magnitude greater than laboratory ones, the computer glass transition temperature lies considerably above the calorimetric one. This is true for a broad range of materials independent of the form of the interaction potential and is consistent with both the universality and "kinetic" nature of the laboratory glass transition. T_g represents the temperature at which the structural relaxation time of the material is comparable to the timescale of experimental measurement. Although numerical values for the calorimetric and computer glass points are different, the working hypothesis adopted here is that the MD simulations provide nanoscale insight into the meaning of for the glass transition.

Changes in the structure of amorphous $\text{CaAl}_2\text{Si}_2\text{O}_8$ with temperature appear insignificant around T_g . The O-O partial static structure factor as well as a detailed analysis of short range coordination statistics for all atoms about all other atoms provide no evidence for a growing static length scale near T_g . The glass transition is clearly a dynamical rather than static structural transition. Indeed, the increase in the structural relaxation time, as reflected by the enormous increase in shear viscosity around T_g is a universal feature of the glass transition. Unlike the concept of a growing static length scale on approach to T_g ,

a growing dynamical length scale can not be ruled out and, in fact, most likely can be found by further analysis of MD-generated atomic trajectories and correlations (e.g., see Morgan and Spera unpublished manuscript, 2001).

There are several means of estimating the computer glass transition. Measures include macroscopic ones such as the change in isobaric heat capacity at T_g defined by a “break” in slope of the H - T relation, the temperature at which speciation equilibria fall out of thermodynamic equilibrium and by analysis of atomic mobility based on tracer diffusion studies. Significantly, all measures provide an estimate of $T_g \approx 2800 \pm 200$ K for the glass transition temperature at 1 GPa for $\text{CaAl}_2\text{Si}_2\text{O}_8$.

The MD simulations provide evidence for the cooperative nature of thermally activated diffusion in both molten and glassy $\text{CaAl}_2\text{Si}_2\text{O}_8$. The small range in both tracer diffusivity (within factor of ~ 2) and activation energy (170–190 kJ/mol) at fixed temperature for Ca, O, Si and Al is consistent with cooperative dynamics. The accessibility of jump sites for Ca is controlled by relaxation of the O-Si-Al network. This represents the mechanism of coupling between O and Ca mobility.

In summary, the MD simulations support the following qualitative view of atom mobility. Supercooled liquids, by virtue of their high densities, possess strong constraints on the frustration dynamics of individual atoms. As temperature decreases toward T_g , a tagged atom is more likely to be trapped by neighbors (i.e., caged) since the amplitude of thermodynamic fluctuations (e.g., internal energy, kinetic energy, etc.) decrease as temperature decreases. Near T_g , a caged particle may remain trapped at a particular site for relatively long times. Liberation of the imprisoned particle requires cooperative rearrangement of several atoms surrounding the tagged particle since neighboring atoms making up the cage are themselves caged and must move as well. In a multicomponent network material like $\text{CaAl}_2\text{Si}_2\text{O}_8$, topological frustration is enhanced by the presence of particles of different effective size and charge. The spatial extent or volume over which cooperative motions must occur to relax a cage dramatically increases as the temperature decreases. Long times are required for cooperative rearrangements involving large numbers of atoms. It is suggested that structural relaxation occur through the motion of groups (mesoscale?) of relatively few, cooperatively moving atoms that cluster or organize spatially in three-dimensional (Euclidean) space. These cooperatively rearranging regions may relax independently from each other at different rates leading to non-Debye relaxation. The precise relationship between this “dynamic heterogeneity” and the cooperatively rearranging regions remains unclear. Detailed studies are now being extended to multicomponent silicate melts of geochemical importance and we are optimistic about the chances for success.

ACKNOWLEDGMENTS

Support from the National Science Foundation (Sonia Esperanza) and the U.S. Department of Energy (Nick Woodward) is gratefully acknowledged. Reviews by K. Binder and an anonymous referee have been most helpful. Technical support from Dean Nevins and Julie Bryce was helpful in the early stages of this work.

REFERENCES CITED

Akaogi, M. (2000) Clues from a shocked meteorite. *Science*, 287, 1602–1603.
 Allen, M.P. and Tildesley, D.J. (1987) *Computer simulation of liquids*, 385 p. Ox-

ford University Press, New York.
 Angell, C.A. (1985) Strong and fragile liquids. In K. Ngai and G.B. Wright, Eds., *Relaxation in Complex Systems*, p. 3–11 National Technical Information Service, U.S. Dept. of Commerce, Springfield, IL.
 ——— (1988) Perspectives on the glass transition. *Journal of Physical Chemistry*, 49, 863–871.
 ——— (1991) Relaxation in liquids, polymers and plastic crystals—strong/fragile patterns and problems. *Journal of Non-Crystalline Solids*, 131, 13–31.
 ——— (1995) Formation of glasses from liquids and biopolymers. *Science*, 267, 1924–1935.
 Angell, C.A., Ngai, K.L., Kieffer, J., Egami, T., and Nienhaus, G.U., Eds. (1997) *Structures and dynamics of glasses and glass formers*, 517 p. Materials Research Society Symposium Proceedings. Pittsburgh, Pennsylvania.
 Bandfield, J.L., Hamilton, V.E., and Christensen, P.R. (2000) A global view of Martian surface compositions from MGS-TES. *Science*, 287, 1626–1630.
 Bansal, N.P. and Doremus, R.H. (1986) *Handbook of glass properties*, 680 p. Academic, San Diego, California.
 Binder, K., Ed. (1995) *Monte Carlo and molecular dynamics simulations in polymer science*. 587 p. Oxford University Press, New York.
 Boon, J.P. and Yip, S. (1980) *Molecular hydrodynamics*, 417 p. McGraw-Hill, New York.
 Bottinga, Y. (1994) Configurational entropy and the non-Newtonian rheology of homogeneous silicate melts. *Physical Review B*, 49, 95–99.
 Bottinga, Y., Richet, P., and Sipp, A. (1995) Viscosity regimes of homogeneous silicate melts. *American Mineralogist*, 80, 305–318.
 Brawer, S. (1985) *Relaxation in viscous liquids and glasses*, 220 p. American Ceramic Society, Columbus, Ohio.
 Bryce, J.G., Spera, F.J., and Stein, D.J. (1999) Pressure dependence of self-diffusion in the NaAlO_2 - SiO_2 system: Compositional effects and mechanisms. *American Mineralogist*, 84, 345–356.
 Debenedetti, P.G. (1996) *Metastable liquids: concepts and principles*, 411 p. Princeton University Press, Princeton, New Jersey.
 Della Valle, R.G. and Andersen, H.C. (1992) Molecular dynamics simulation of silica liquid and glass. *Journal of Chemical Physics*, 97, 2682–2689.
 Dingwell, D.B. (1995) Relaxation in silicate melt: Some applications. In J.F. Stebbins, P.F. McMillan, and D.B. Dingwell, Eds., *Structure, Dynamics and Properties of Silicate Melts*, 32, p. 21–66. Reviews in Mineralogy, Mineralogical Society of America, Washington, D.C.
 Dingwell, D.B. and Webb, S.L. (1990) Relaxation in silicate melts. *European Journal of Mineralogy*, 2, 427–449.
 Downs, R.T., Hazen, R.M., Finger, L.W., and Gasparik, T. (1995) Crystal chemistry of lead aluminosilicate hollandite—A new high-pressure synthetic phase with octahedral Si. *American Mineralogist*, 80, 937–940.
 Ediger, M.D. (1996) Supercooled liquids and glasses. *Journal of Physical Chemistry*, 100, 13200–13212.
 Fredrickson, G.H. (1988) Recent developments in dynamical theories of the liquid-glass transition. *Annual Review of Physical Chemistry*, 39, 149–180.
 Fodor, R.V., Jacobs, R.S., and Bauer, G.R. (1994) Hollandite in Hawaiian basalt—a relocation site for weathering-mobilized elements. *Mineralogical Magazine*, 58, 589–596.
 Hansen, J.P. and McDonald, I.R. (1986) *Theory of simple liquids*, 556 p. Academic, New York.
 Hess, K.-U. and Dingwell, D.B. (1995) The influence of excess alkalis on the viscosity of a haplogranitic melt. *American Mineralogist*, 80, 297–304.
 Horbach, J. and Kob, W. (1999) Static and dynamic properties of viscous silica melt. *Physical Review B*, 60, 3169–3181.
 Hummel, W. and Arndt, J. (1985) Variation of viscosity with temperature and composition in the plagioclase system. *Contributions to Mineralogy and Petrology*, 90, 83–92.
 Kob, W. (1995) Computer simulations of supercooled liquids and structural glasses. *Annual Reviews of Computational Physics*, 3, 1–43.
 ——— (1999) Computer simulations of supercooled liquids and glasses. *Journal of Physics: Condensed Matter*, 11, R85–R115.
 Leshar, C.E., Hervig, R.L., and Tinker, D. (1996) Self diffusion of network formers (silicon and oxygen) in naturally occurring basaltic liquid. *Geochemica et Cosmochimica Acta*, 60, 405–413.
 Maekawa, H., Maekawa, T., Kawamura, K., and Yokokawa, T. (1991) The structural groups of alkali silicate glasses determined from ^{29}Si MAS-NMR. *Journal of Non-Crystalline Solids*, 127, 53–64.
 McMillan, P.F. and Wolf, G.H. (1995) Vibrational spectroscopy of silicate liquids. In J.F. Stebbins, P.F. McMillan, and D.B. Dingwell, Eds., *Structure, Dynamics and Properties of Silicate Melts*, 32, p. 247–315. Mineralogical Society of America, Washington, D.C.
 Morse, S.A. (1980) *Basalts and phase diagrams*, 245 p. Springer-Verlag, New York.
 Moynihan, C.T. (1995) Structural relaxation and the glass transition. In J.F. Stebbins, P.F. McMillan, and D.B. Dingwell, Eds., *Structure, Dynamics and Properties of Silicate Melts*, 32, p. 1–19. Mineralogical Society of America, Washington, D.C.
 Moynihan, C.T., Easteal, A.J., DeBolt, M.A., and Tucker, J. (1976) Dependence of fictive temperature of glass on cooling rate. *Journal of the American Ceramic*

- Society, 59, 12–16.
- Navrotsky, A. (1995) Energetics of silicate melts. In J.F. Stebbins, P.F. McMillan, and D.B. Dingwell, Eds., *Structure, Dynamics and Properties of Silicate Melts*, 32, p. 121–143. Mineralogical Society of America, Washington, D.C.
- Nevins, D. and Spera, F.J. (1998) Molecular dynamics simulations of molten $\text{CaAl}_2\text{Si}_2\text{O}_8$: Dependence of structure and properties on pressure. *American Mineralogist*, 83, 1220–1230.
- Ogawa, H., Shiraiishi, Y., Kawamura, K., and Yokokawa, T. (1990) Molecular dynamics study on the shear viscosity of molten $\text{Na}_2\text{O}\cdot 2\text{SiO}_2$. *Journal of Non-Crystalline Solids*, 119, 151–158.
- Pakula, T. and Teichmann, J. (1997) A model for relaxation in supercooled liquids and polymer melts. In C.A. Angell, K.L. Ngai, J. Kieffer, T. Egami, and G.U. Nienhaus, Eds., *Structures and Dynamics of Glasses and Glass Formers*, 455, 211–222. Materials Research Society Symposium Proceedings, Pittsburgh, Pennsylvania.
- Ramano, C., Dingwell, D.B., and Behrens, H. (1995) The temperature dependence of the speciation of water in $\text{NaAlSi}_3\text{O}_8$ - KAlSi_3O_8 melts—An application of fictive temperatures derived from synthetic fluid inclusions. *Contributions to Mineralogy and Petrology*, 122, 1–10.
- Richet, P. and Bottinga, Y. (1984a) Glass transitions and thermodynamic properties of amorphous SiO_2 , $\text{NaAlSi}_3\text{O}_8$, and KAlSi_3O_8 . *Geochemica et Cosmochemica Acta*, 48, 453–470.
- (1984b) Anorthite, andesine, wollastonite, diopside, cordierite and pyrope: thermodynamics of melting, glass transitions, and properties of the amorphous phases. *Earth and Planetary Science Letters*, 67, 415–432.
- (1995) Rheology and configurational entropy of silicate melts. In J.F. Stebbins, P.F. McMillan, and D.B. Dingwell, Eds., *Structure, Dynamics and Properties of Silicate Melts*, 32, p. 67–93. Reviews in Mineralogy, Mineralogical Society of America, Washington, D.C.
- Rustad, J.R., Yuen, D.A., and Spera, F.J. (1990) Molecular Dynamics of liquid SiO_2 under high pressure. *Physical Review A*, 42, 2081–2089.
- (1991a) The sensitivity of physical and spectral properties of silica glass to variations of interatomic potentials under high pressure. *Physics of the Earth and Planetary Interiors*, 65, 210–230.
- (1991b) The statistical geometry of pressure-induced coordination modifications in amorphous silica. *Eos*, 72, 146.
- (1991c) The statistical geometry of amorphous silica at lower mantle pressures; implications for melting slopes of silicates and anharmonicity. *Journal of Geophysical Research*, B, Solid Earth and Planets, 96, 19665–19673.
- (1992) Coordination variability and the structural components of silica glass under high pressures. *Chemical Geology*, 96, 421–437.
- Scamehorn, C.A. and Angell, C.A. (1991) Viscosity-temperature relations and structure in fully polymerized aluminosilicate melts from ion dynamics simulations. *Geochemica et Cosmochemica Acta*, 55, 721–730.
- Scherer, G.W. (1986) *Relaxation in glasses and composites*, 331 p. Wiley, New York.
- Stebbins, J.F. (1995) Dynamics and structure of silicate and oxide melts: Nuclear magnetic resonance studies. In J.F. Stebbins, P.F. McMillan, and D.B. Dingwell, Eds., *Structure, Dynamics and Properties of Silicate Melts*, 32, p. 191–246. Mineralogical Society of America, Washington, D.C.
- Stebbins, J.F. and Poe, B.T. (1999) Pentacoordinate silicon in high-pressure crystalline and glassy phases of calcium disilicate (CaSi_2O_6). *Geophysical Research Letters*, 26, 2521–2523.
- Stebbins, J.F., McMillan, P.F., and Dingwell, D.B., Eds. (1995) *Structure, Dynamics, and Properties of Silicate Melts*, 616 p. Mineralogical Society of America, Washington D.C.
- Stein, D.J. and Spera, F.J. (1995) Molecular dynamics simulations of liquids and glasses in the system $\text{NaAlSi}_3\text{O}_8$ - SiO_2 : I: Methodology and melt structures. *American Mineralogist*, 80, 417–431. potential of silica applied to molecular dynamics. *Physical Review Letters*, 61, 869–872.
- Stein, D.J. and Spera, F.J. (1996) Molecular Dynamics simulations of liquids and glasses in the system $\text{NaAlSi}_3\text{O}_8$ - SiO_2 : Physical Properties and transport mechanisms. *American Mineralogist*, 81, 284–302.
- Tsuneyuki, S., Tsukada, M., Aoki, H., and Matsui, Y. (1988) First principles interatomic potential of silica applied to molecular dynamics. *Physical Review Letters*, 61, 869–872.
- Urbain, G., Bottinga, Y., and Richet, P. (1982) Viscosity of liquid silica, silicates and aluminosilicates. *Geochemica et Cosmochemica Acta*, 46, 1061–1072.
- van Beest, B.W.H., Kramer, G.J., and van Santen, R.A. (1990) Force fields for silicates and aluminophosphates based on *ab initio* calculations. *Physical Review Letters*, 64, 1955–1958.
- Vollmayr, K., Kob, W., and Binder, K. (1996) Cooling-rate effects in amorphous silica: A computer-simulation study. *Physical Review B*, 54, 15808–15827.
- Zallen, R. (1983) *The physics of amorphous solids*, 316 p. Wiley-Interscience, New York.
- Zarzycki, J. (1991) *Glasses and the vitreous state*, 505 p. Cambridge University Press, New York.
- Zhang, J.M., Ko, J.D., Hazen, R.M., and Prewitt, C.T. (1993) High pressure crystal chemistry of KAlSi_3O_8 hollandite. *American Mineralogist*, 78, 493–499.

MANUSCRIPT RECEIVED AUGUST 14, 2000

MANUSCRIPT ACCEPTED MARCH 12, 2001

MANUSCRIPT HANDLED BY BJOERN WINKLER